Relativistic cross sections of the electron-impact ionization of heliumlike ions

Tien-Yow Kuo[1] and Keh-Ning Huang[2,3]
[1]*Institute of Optoelectronic Sciences, National Taiwan Ocean University, Keelung, Taiwan 202, Republic of China*
[2]*Department of Physics, National Taiwan University, Taipei, Taiwan 106, Republic of China*
[3]*Institute of Atomic and Molecular Sciences, Academia Sinica, P. O. Box 23-166, Taipei, Taiwan 106, Republic of China*
(Received 5 February 2001; published 17 August 2001)

Single-differential and total cross sections of electron-impact ionization are calculated in a relativistic formulation for ions in the helium isoelectronic sequence: He, Li^+, B^{3+}, C^{4+}, N^{5+}, Na^{9+}, Fe^{24+}, and Ag^{45+}. Transition amplitudes are evaluated in the two-potential distorted-wave approximation. Relativistic effects are investigated by taking the nonrelativistic limit. Both the rearrange and capture amplitudes are found to be important near the ionization threshold. Results are compared with other theoretical calculations and experimental data. The systematics of ionization cross sections along the isoelectronic sequence is also studied.

DOI: 10.1103/PhysRevA.64.032710 PACS number(s): 34.80.Dp

I. INTRODUCTION

Electron-impact ionization is the major mode of ionization processes in the fusion plasma, besides being of fundamental interest in atomic structure and collision mechanisms. In particular, knowledge of ionization cross sections has applications in astrophysics, plasma physics, and radiation physics. Earlier reviews of electron-impact ionization of atoms were given by McCarthy and Weigold [1] and by Mark and Dunn [2], and a compilation of experimental and selected theoretical data was given by Tawara and Kato [3].

The ionization cross section for C^{4+} was obtained by Beigman and Vainshtein [4] in the Coulomb-Born approximation. Total cross sections were calculated using the Born approximation by Bell and Kingston [5] for He, and by Economides and McDowell [6] for He and Li^+. The total cross section for Li^+ was given by Moores and Nussbaumer [7] in the no-exchange Coulomb-Born approximation. Burgess *et al.* [8] had studied the electron-impact ionization of highly charged ions in the exchange-classical-impact-parameter method. Single-differential and total cross sections of He were computed by Bransden *et al.* [9] in the distorted-wave polarized-orbital method, which includes static exchange and polarization potential. Younger [10,11] performed the parametrized distorted-wave calculations for He, Li^+, B^{3+}, C^{4+}, N^{5+}, Na^{9+}, and Fe^{24+} . More recent theoretical cross sections for heliumlike ions were given by Kim and Rudd [12] in a semiempirical model, which combines the binary-encounter theory with the dipole interaction of the Bethe theory for fast incident electrons. Single-differential and total cross sections for He were calculated by Biswas and Sinha [13] in the correlated three-body Coulomb continuum method, including the electron-exchange effect. Fontes *et al.* [14] studied $1s$ ionization cross sections for a variety of ions with one to four bound electrons and nuclear charge Z in the range of $10 \leqslant Z \leqslant 92$ within the relativistic distorted-wave approximation including the generalized Breit interaction. The total cross section for Li^+ was calculated by Pindzola *et al.* [15] in the R-matrix method with pseudostates and time-dependent close coupling.

Measurements of single-differential cross sections for He were made by Grissom *et al.* [16], Opal *et al.* [17], Crooks [18], and Shyn and Sharp [19]. Total cross sections for He were measured by Smith [20], Schram *et al.* [21], Brook *et al.* [22], Montague *et al.* [23], and Shah *et al.* [24]. Total cross sections for Li^+ were measured by Lineberger *et al.* [25], Wareing and Dolder [26], and Peart and Dolder [27]. Crandall *et al.* [28] measured the total cross sections for C^{4+} and N^{5+}.

A complete theoretical kinematic analysis of the electron-impact ionization process [29] and electron-atom scatterings [30], in general, has been presented by Huang in the relativistic formulation. We have computed transition amplitudes of the electron-impact ionization process in the two-potential distorted-wave (TPDW) approximation with exact exchange effects. The applications of the TPDW to the electron-impact and positron-impact ionizations of hydrogenlike and heliumlike ions have been reported [31–36]. In this paper we shall present ionization cross sections for He, Li^+, B^{3+}, C^{4+}, N^{5+}, Na^{9+}, Fe^{24+}, and Ag^{45+} in the helium isoelectronic sequence, which have been given earlier only in a Ph.D. thesis [31]. Both the rearrange and capture amplitudes are found to be important compared to the direct amplitude at low incident energies for light ions.

In Sec. II, we shall review the general theory of electron-impact ionization and two-potential distorted-wave approximation. We express transition amplitudes in terms of radial integrals and outline the numerical method in Sec. III. In Sec. IV, we compare our results with experiment and with other theoretical results. The conclusion is made in Sec. V.

II. THEORY

A. Kinematic analysis

In the electron-impact ionization processes, we denote the linear momentum and total energy of the incident electron by $\mathbf{k}_i$ and E_i, respectively. Before the collision, the heliumlike ion is in its ground state. After the collision, one electron of the ion is ejected, and the residual hydrogenic ion is left in its ground state. The two outgoing electrons are described by $(\mathbf{k}_p E_p)$ and $(\mathbf{k}_s E_s)$, where the primary electron is defined as the faster one with subscript p, and the secondary electron as the slower one with subscript s.

By energy conservation, we have

$$E_i + E_b = E_p + E_s, \tag{1}$$

where E_b is the energy of the electron originally bound in the heliumlike ion. By scattering theory, we may express the triple-differential cross section as [29]

$$\frac{d^3\sigma}{dE_s d\Omega_p d\Omega_s} = \frac{(2\pi)^4}{c^6}\left(\frac{k_p E_p k_s E_s E_i}{k_i}\right)|T_{fi}|^2, \tag{2}$$

where T_{fi} denotes symbolically the transition matrix element. By integrating the triple-differential cross sections over Ω_p and Ω_s, we obtain the following expression for the single-differential cross section:

$$\frac{d\sigma}{dE_s} = \frac{2\pi^3}{k_i^2(2J_0+1)}\overline{\sigma}, \tag{3}$$

where J_0 is the total-angular-momentum quantum number of the target ion, and

$$\overline{\sigma} = \sum_\alpha d_\alpha^2. \tag{4}$$

Here the summation is over all possible channels symbolically denoted by the index $\alpha \equiv (\kappa_i, \kappa_p, \kappa_s, j, J)$, and the real amplitude d_α is defined by the reduced matrix element of the partial-wave amplitude in channel α, i.e.,

$$d_\alpha \exp(i\delta_\alpha) = i^{l_i-(l_p+l_s)} \exp[i(\sigma_{k_p}+\sigma_{k_s})] \times \langle \alpha^-[J_\alpha(j_p j_s)J] \| H_I \| (J_0 j_i)J\rangle, \tag{5}$$

where H_I denotes symbolically the appropriate interaction.

The total cross section can be calculated as

$$\sigma = \int_{mc^2}^{(E_i+E_b)/2} \frac{d\sigma}{dE_s} dE_s, \tag{6}$$

where mc^2 is the rest energy of the electron, and c is the speed of light.

B. Two-potential distorted-wave approximation

In our case, the total Hamiltonian H for electrons in the composite system of projectile and target is assumed to be, in atomic units, $m = e = \hbar = 1$,

$$H = (c\boldsymbol{\alpha}_1\cdot\mathbf{p}_1 + c^2\beta_1) + (c\boldsymbol{\alpha}_2\cdot\mathbf{p}_2 + c^2\beta_2) + (c\boldsymbol{\alpha}_3\cdot\mathbf{p}_3 + c^2\beta_3) - \frac{Z}{r_1} - \frac{Z}{r_2} - \frac{Z}{r_3} + \frac{1}{r_{12}} + \frac{1}{r_{13}} + \frac{1}{r_{23}}, \tag{7}$$

where $\boldsymbol{\alpha}_i$ and β_i are Dirac matrices, and Z is the charge of the nucleus. The speed of light c equals the inverse of the fine-structure constant in atomic units.

The total Hamiltonian can be separated into two parts,

$$H = H_i + V_i, \tag{8}$$

where H_i is the unperturbed Hamiltonian and V_i is the interaction potential, and

$$H_i = (c\boldsymbol{\alpha}_1\cdot\mathbf{p}_1 + c^2\beta_1) + (c\boldsymbol{\alpha}_2\cdot\mathbf{p}_2 + c^2\beta_2) + (c\boldsymbol{\alpha}_3\cdot\mathbf{p}_3 + c^2\beta_3) - \frac{Z}{r_2} - \frac{Z}{r_3} + \frac{1}{r_{23}}, \tag{9}$$

$$V_i = -\frac{Z}{r_1} + \frac{1}{r_{12}} + \frac{1}{r_{13}}. \tag{10}$$

Here r_1, r_2, and r_3 refer to the spatial coordinates of the incident electron and two bound electrons before the collision and those of the primary, secondary, and bounded electrons, respectively, after the collision.

By considering antisymmetrization, the transition matrix element will have exchange terms in addition to the usual direct term. In the prior form, it is given by [37]

$$T_{fi} = \langle \Psi_f^{(-)}|V_i|\Phi_i\rangle - \langle P\Psi_f^{(-)}|V_i|\Phi_i\rangle, \tag{11}$$

where Φ_i is the eigenstate of H_i, and $\Psi_f^{(-)}$ is the eigenstate of H with the incoming-wave boundary condition. Here P denotes the permutation of the coordinate of the primary electron with those of the secondary and bound electrons.

In the two-potential formulation, the interaction potential may be split as

$$V_i = U_i + W_i. \tag{12}$$

Because in the initial state the incident electron is screened by the bound electrons, we may well choose

$$U_i = -\frac{Z}{r_1} + \nu_i(r_1), \tag{13}$$

$$W_i = \frac{1}{r_{12}} + \frac{1}{r_{13}} - \nu_i(r_1), \tag{14}$$

where $\nu_i(r_1)$ is the average potential due to the bound electrons in the heliumlike ion, i.e.,

$$\nu_i(r_1) = \left\langle \Phi(\mathbf{r}_2,\mathbf{r}_3)\left|\frac{1}{r_{12}} + \frac{1}{r_{13}}\right|\Phi(\mathbf{r}_2,\mathbf{r}_3)\right\rangle. \tag{15}$$

Here the ground-state wave function $\Phi(\mathbf{r}_2,\mathbf{r}_3)$ for the heliumlike ion is approximated by

$$\Phi(\mathbf{r}_2,\mathbf{r}_3) = \frac{1}{\sqrt{2}}[\Phi_b(\mathbf{r}_2)\Phi_{b'}(\mathbf{r}_3) - \Phi_b(\mathbf{r}_3)\Phi_{b'}(\mathbf{r}_2)], \tag{16}$$

where Φ_b and $\Phi_{b'}$ denote the wave functions for the bound electrons in the heliumlike ion, and the prime denotes a difference in the magnetic quantum number. The bound-electron wave functions were calculated with the multiconfiguration relativistic Dirac-Fock program by Desclaux [38]. Therefore, the potential $\nu_i(r_1)$ in Eq. (15) can be reduced to

$$\nu_i(r_1)=2\left\langle \Phi_b(\mathbf{r}_3)\left|\frac{1}{r_{13}}\right|\Phi_b(\mathbf{r}_3)\right\rangle. \tag{17}$$

We take the potential U_i in Eq. (13) to be the distorting potential for the incident electron such that the distorted wave function $\chi_i^{(+)}$ with the outgoing-wave boundary condition satisfies the equation

$$(c\boldsymbol{\alpha}_1\cdot\mathbf{p}_1+c^2\beta_1+U_i-E_i)\chi_i^{(+)}(\mathbf{r}_1)=0. \tag{18}$$

After some algebra, the transition matrix element (11) becomes [31]

$$T_{fi}=\langle\Psi_f^{(-)}|W_i|\psi_i^{(+)}\rangle-\langle P\Psi_f^{(-)}|W_i|\psi_i^{(+)}\rangle, \tag{19}$$

where $\psi_i^{(+)}$ is the unsymmetrized wave function, given as

$$\psi_i^{(+)}=\chi_i^{(+)}(\mathbf{r}_1)\Phi_b(\mathbf{r}_2)\Phi_{b'}(\mathbf{r}_3). \tag{20}$$

To find an approximation to the final-state wave function $\Psi_f^{(-)}$ with the incoming-wave boundary condition, we choose the distorted final-state wave function as

$$\Psi_f^{(-)}=\chi_p^{(-)}(\mathbf{r}_1)\chi_s^{(-)}(\mathbf{r}_2)\Phi_0(\mathbf{r}_3). \tag{21}$$

Here Φ_0 denotes the ground-state wave function for the bound electron in the hydrogenic ion, and $\chi_p^{(-)}$ and $\chi_s^{(-)}$ satisfy the following equations:

$$(c\boldsymbol{\alpha}_1\cdot\mathbf{p}_1+c^2\beta_1+U_p-E_p)\chi_p^{(-)}(\mathbf{r}_1)=0, \tag{22}$$

TABLE I. Distorting potentials and asymptotic charges for the primary and secondary electrons in models TPDW01, TPDW11, and TPDW00.

Model	Distorting potential U_p	Distorting potential U_s	Asymptotic charges Z_p	Asymptotic charges Z_s
TPDW01	$-\frac{Z}{r_1}+\nu_i(r_1)$	$-\frac{Z}{r_2}+\nu_f(r_2)$	$Z-2$	$Z-1$
TPDW11	$-\frac{Z}{r_1}+\nu_f(r_1)$	$-\frac{Z}{r_2}+\nu_f(r_2)$	$Z-1$	$Z-1$
TPDW00	$-\frac{Z}{r_1}+\nu_i(r_1)$	$-\frac{Z}{r_2}+\nu_i(r_2)$	$Z-2$	$Z-2$

$$(c\boldsymbol{\alpha}_2\cdot\mathbf{p}_2+c^2\beta_2+U_s-E_s)\chi_s^{(-)}(\mathbf{r}_2)=0. \tag{23}$$

We summarize in Table I, the distorting potentials U_p and U_s for the primary and secondary electrons, respectively, in the three models used in the present calculation. In Table I, ν_f denotes the average potential arising from the bound electron in the residual hydrogenic ion,

$$\nu_f(r_k)=\left\langle \Phi_0(\mathbf{r}_3)\left|\frac{1}{r_{k3}}\right|\Phi_0(\mathbf{r}_3)\right\rangle. \tag{24}$$

The transition matrix element (19) can then be written as

$$T_{fi}=D_{fi}-R_{fi}+C_{fi}, \tag{25}$$

where D_{fi}, R_{fi}, and C_{fi} are called the direct, rearrange, and capture terms, respectively, and the rearrange and capture terms are due to the exchange effects. These terms are given explicitly as follows.

(i) Direct term

$$D_{fi}=\sqrt{2}\left\langle \chi_p^{(-)}(\mathbf{r}_1)\chi_s^{(-)}(\mathbf{r}_2)\Phi_0(\mathbf{r}_3)\left|\frac{1}{r_{12}}+\frac{1}{r_{13}}-\nu_i(r_1)\right|\chi_i^{(+)}(\mathbf{r}_1)\Phi_b(\mathbf{r}_2)\Phi_{b'}(\mathbf{r}_3)\right\rangle, \tag{26}$$

(ii) Rearrange term

$$R_{fi}=\sqrt{2}\left\langle \chi_p^{(-)}(\mathbf{r}_2)\chi_s^{(-)}(\mathbf{r}_1)\Phi_0(\mathbf{r}_3)\left|\frac{1}{r_{12}}+\frac{1}{r_{13}}-\nu_i(r_1)\right|\chi_i^{(+)}(\mathbf{r}_1)\Phi_b(\mathbf{r}_2)\Phi_{b'}(\mathbf{r}_3)\right\rangle, \tag{27}$$

(iii) Capture term

$$C_{fi}=\sqrt{2}\left\langle \chi_p^{(-)}(\mathbf{r}_3)\chi_s^{(-)}(\mathbf{r}_2)\Phi_0(\mathbf{r}_1)\left|\frac{1}{r_{12}}+\frac{1}{r_{13}}-\nu_i(r_1)\right|\chi_i^{(+)}(\mathbf{r}_1)\Phi_b(\mathbf{r}_2)\Phi_{b'}(\mathbf{r}_3)\right\rangle. \tag{28}$$

III. NUMERICAL METHOD

Using a graphical method [39], we can easily express the transition amplitude as

$$d_\alpha=\left\langle\frac{1}{r_{12}}\right\rangle_d+\left\langle\frac{1}{r_{13}}\right\rangle_d-\langle\nu_i\rangle_d-\left\langle\frac{1}{r_{12}}\right\rangle_r-\left\langle\frac{1}{r_{13}}\right\rangle_r+\langle\nu_i\rangle_r+\left\langle\frac{1}{r_{12}}\right\rangle_c+\left\langle\frac{1}{r_{13}}\right\rangle_c-\langle\nu_i\rangle_c, \tag{29}$$

where

$$\left\langle\frac{1}{r_{12}}\right\rangle_d=\sqrt{2}(-1)^{j_s+j+1/2}[jj_ij_pj_s]\begin{pmatrix}\frac{1}{2} & l_s & j_s\\ \frac{1}{2} & 0 & -\frac{1}{2}\end{pmatrix}\times\begin{pmatrix}j_i & l_s & j_p\\ \frac{1}{2} & 0 & -\frac{1}{2}\end{pmatrix}\times\begin{Bmatrix}j_p & j_s & j\\ \frac{1}{2} & j_i & l_s\end{Bmatrix}\langle W_{0b}\rangle\times\langle W_{b's}R_{l_s}W_{ip}\rangle^{even}, \tag{30}$$

$$\left\langle\frac{1}{r_{13}}\right\rangle_d=2(-1)^{2j_i+j}[jj_ij_p]\begin{pmatrix}\frac{1}{2} & 0 & \frac{1}{2}\\ \frac{1}{2} & 0 & -\frac{1}{2}\end{pmatrix}\times\begin{pmatrix}j_i & 0 & j_p\\ \frac{1}{2} & 0 & -\frac{1}{2}\end{pmatrix}\times\begin{Bmatrix}j_p & j_s & j\\ \frac{1}{2} & j_i & 0\end{Bmatrix}\langle W_{sb'}\rangle\times\langle W_{b0}R_0W_{ip}\rangle^{even}, \tag{31}$$

$$\langle\nu_i\rangle_d=[j]\{j_pj_sj\}\langle W_{0b}\rangle\langle W_{sb'}\rangle\langle W_{pi}\nu_i\rangle, \tag{32}$$

$$\left\langle\frac{1}{r_{12}}\right\rangle_r=-\sqrt{2}(-1)^{j_s+1/2}[jj_ij_pj_s]\begin{pmatrix}\frac{1}{2} & l_p & j_p\\ \frac{1}{2} & 0 & -\frac{1}{2}\end{pmatrix}\times\begin{pmatrix}j_i & l_p & j_s\\ \frac{1}{2} & 0 & -\frac{1}{2}\end{pmatrix}\times\begin{Bmatrix}j_p & j_s & j\\ j_i & \frac{1}{2} & l_p\end{Bmatrix}\langle W_{0b}\rangle\times\langle W_{b'p}R_{l_p}W_{is}\rangle^{even}, \tag{33}$$

$$\left\langle\frac{1}{r_{13}}\right\rangle_r=2(-1)^{j_s}[jj_ij_s]\begin{pmatrix}\frac{1}{2} & 0 & \frac{1}{2}\\ \frac{1}{2} & 0 & -\frac{1}{2}\end{pmatrix}\begin{pmatrix}j_i & 0 & j_s\\ \frac{1}{2} & 0 & -\frac{1}{2}\end{pmatrix}\times\begin{Bmatrix}j_p & j_s & j\\ j_i & \frac{1}{2} & 0\end{Bmatrix}\langle W_{pb'}\rangle\langle W_{b0}R_0W_{is}\rangle^{even}, \tag{34}$$

$$\langle\nu_i\rangle_r=(-1)^{j+j_i+j_p}[j]\{j_pj_sj\}\langle W_{0b}\rangle\langle W_{pb'}\rangle\langle W_{si}\nu_i\rangle, \tag{35}$$

$$\left\langle\frac{1}{r_{12}}\right\rangle_c=-2\,\delta_{\lambda j}\delta_{\lambda l_s}\delta_{\lambda l_i}(-1)^{j+j_p+j_s}[j]^{-1}[j_ij_s]\{j_ij_0j\}\times\{j_pj_sj\}\times\begin{pmatrix}\frac{1}{2} & \lambda & j_s\\ \frac{1}{2} & 0 & -\frac{1}{2}\end{pmatrix}\begin{pmatrix}j_i & \lambda & \frac{1}{2}\\ \frac{1}{2} & 0 & -\frac{1}{2}\end{pmatrix}\times\langle W_{pb}\rangle\langle W_{b's}R_\lambda W_{i0}\rangle^{even}, \tag{36}$$

$$\left\langle\frac{1}{r_{13}}\right\rangle_c=-2\,\delta_{\lambda j}\delta_{\lambda l_p}\delta_{\lambda l_i}(-1)^{2j_i}[j]^{-1}[j_ij_p]\{j_ij_0j\}\{j_pj_sj\}\times\begin{pmatrix}\frac{1}{2} & \lambda & j_p\\ \frac{1}{2} & 0 & -\frac{1}{2}\end{pmatrix}\begin{pmatrix}j_i & \lambda & \frac{1}{2}\\ \frac{1}{2} & 0 & -\frac{1}{2}\end{pmatrix}\langle W_{sb'}\rangle\times\langle W_{bp}R_\lambda W_{i0}\rangle^{even}, \tag{37}$$

$$\langle\nu_i\rangle_c=\sqrt{2}(-1)^{2j_s}[j_i]\langle W_{pb}\rangle\langle W_{sb'}\rangle\langle W_{0i}\nu_i\rangle. \tag{38}$$

Here besides *3n-j* symbols and obvious notations [29,31], other notations are defined below,

$$[j]=\sqrt{2j+1},$$

$$\{j_1j_2j_3\}=\begin{cases}1 & \text{if } |j_1-j_2|\leqslant j_3\leqslant|j_1+j_2|\\ 0 & \text{otherwise,}\end{cases} \tag{39}$$

$$R_\lambda(r_1,r_2)=\frac{r_<^\lambda}{r_>^{\lambda+1}}, \tag{40}$$

$$\langle W_{ab}V\rangle=\int_0^\infty dr\,W_{ab}(r)V(r), \tag{41}$$

$$W_{ab}(r)=G_a(r)G_b(r)+F_a(r)F_b(r), \tag{42}$$

$$\langle W_{ab}R_\lambda W_{cd}\rangle^{even}=\pi(l_a\lambda l_b)\pi(l_c\lambda l_d)\int\int_0^\infty dr_1dr_2W_{ab}\times(r_1)R_\lambda(r_1,r_2)W_{cd}(r_2), \tag{43}$$

with the parity function

$$\pi(l_\alpha\lambda l_\beta)=\begin{cases}1, & l_\alpha+\lambda+l_\beta=even\\ 0, & l_\alpha+\lambda+l_\beta=odd.\end{cases}$$

In the electron-impact ionization of heliumlike ions, we have specifically $j_0=j_b=\frac{1}{2}$, $l_0=l_b=0$, and $J=j_i$.

Numerical calculations are carried out for the amplitudes d_α with different choices of distorting potentials for three different models as shown in Table I. To identify relativistic

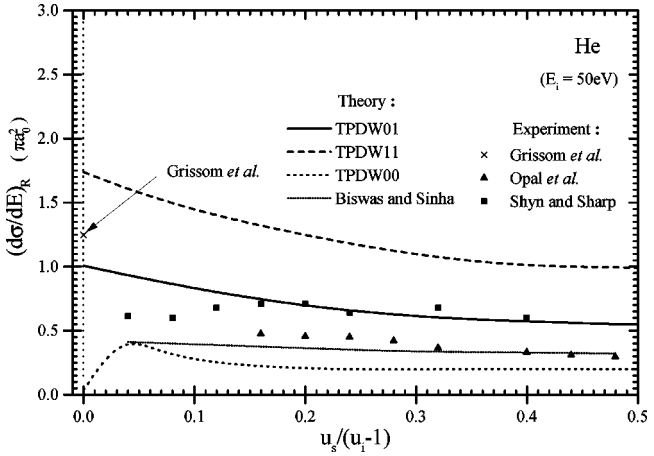

FIG. 1. Reduced single-differential cross sections (in πa_0^2) for He at the incident energy $E_i = 50$ eV.

effects, we calculate the nonrelativistic cross sections by letting the speed of light c go to infinity.

IV. RESULTS AND DISCUSSION

To compare single-differential and total cross sections of different ions, the threshold energy units, $u_i = (E_i - c^2)/I$, $u_p = (E_p - c^2)/I$, and $u_s = (E_s - c^2)/I$ are employed, and reduced cross sections are defined as

$$\left(\frac{d\sigma}{dE_s}\right)_R = \left(\frac{I}{I_{\mathrm{He}}}\right)^3 \frac{d\sigma}{dE_s},$$

$$\sigma_R = \left(\frac{I}{I_{\mathrm{He}}}\right)^2 \sigma,$$

where I denotes the ionization potential of the particular ion in consideration, and I_{He}that of the helium atom.

We have calculated the single-differential cross section for He, the total cross sections for He, Li^+, B^{3+}, C^{4+}, N^{5+}, Na^{9+}, Fe^{24+}, and Ag^{45+} in the helium isoelectronic sequence. In Figs. 1–3, we show the reduced single-differential

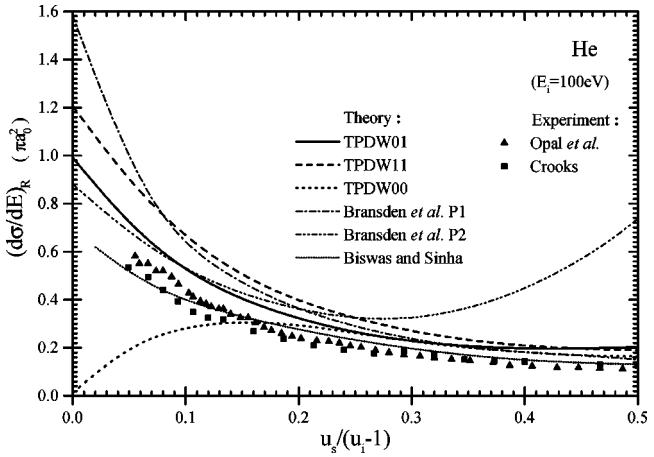

FIG. 2. Reduced single-differential cross sections (in πa_0^2) for He at the incident energy $E_i = 100$ eV.

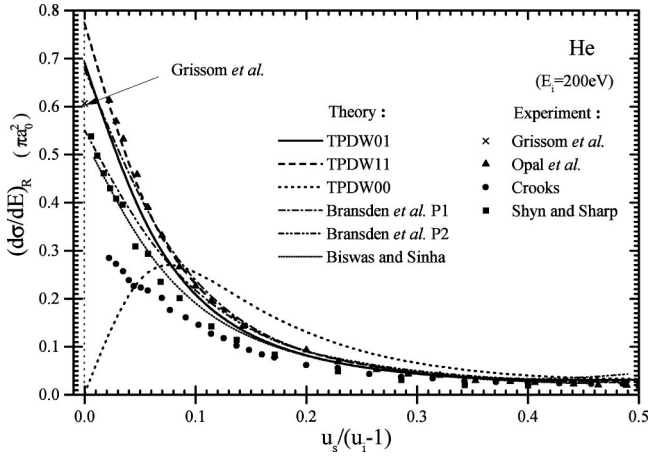

FIG. 3. Reduced single-differential cross sections (in πa_0^2) for He at the incident energy $E_i = 200$ eV. Here the $P1$ curve of Bransden *et al.* is almost indiscernible from our TPDW11 curve except near the threshold.

cross sections for He at $E_i = 50$ eV, 100 eV, and 200 eV, respectively, compared with the theoretical results of Bransden *et al.* [9], and with the experimental data of Grissom *et al.* [16], Opal *et al.* [17], Crooks [18], and Shyn and Sharp [19]. The TPDW01 and TPDW11 curves agree reasonably well with the experimental data. We find the TPDW01 and TPDW11 curves decrease slowly with u_s at low incident energies and decrease rapidly with u_s and converge together at high incident energies, but the TPDW00 curve has quite different characteristics. This is due to the fact that the secondary electron is not completely screened and affected by a long-range Coulomb potential in both the TPDW01 and TPDW11 models, while the secondary electron in the TPDW00 model is completely screened. Furthermore, as can be seen from Figs. 2 and 3, the reduced single-differential cross sections in the TPDW01 and TPDW11 models decrease rapidly as the secondary-electron energies increase. As can be seen from Fig. 3, the total cross section at high incident energies comes mainly from the low secondary electron-energy region of the single-differential cross section.

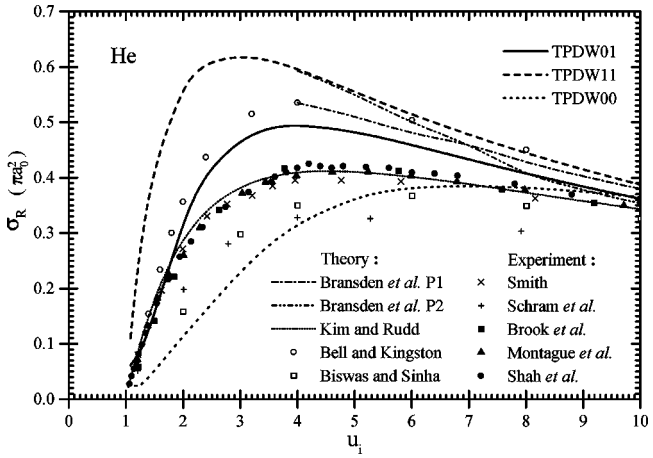

FIG. 4. Reduced total cross sections (in πa_0^2) for He.

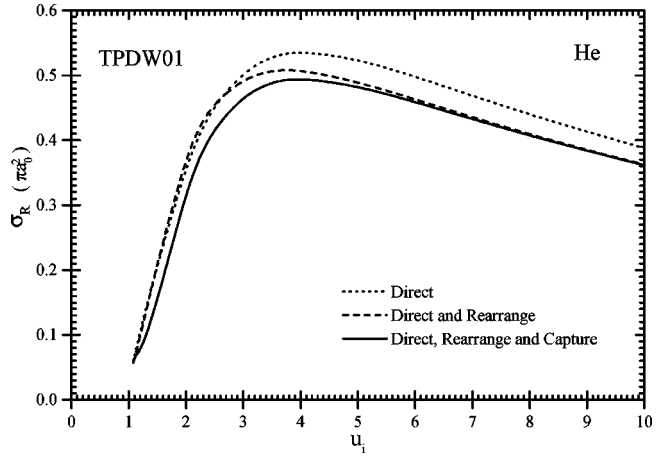

FIG. 5. Reduced total cross sections (in πa_0^2) for He in model TPDW01 with *D* term, DR term, and DRC term, respectively.

In Fig. 4, we present the reduced total cross section for He and compare with the theoretical results of Bell and Kingston [5], Bransden *et al.* [9], Kim and Rudd [12], and Biswas and Sinha [13] and with the experimental data of Smith [20], Schram *et al.* [21], Brook *et al.* [22], Montague *et al.* [23], and Shah *et al.* [24]. The TPDW01 curve is in good agreement with experiment, while the TPDW11 and TPDW00 curves give reasonable results at high incident energies. We show exchange effects in the TPDW01 model for He in Fig. 5. We note that the exchange, including rearrange and capture, terms in the transition amplitudes play an important role, reducing the no-exchange values by 10–30 %. In the low-incident-energy region, the capture amplitude is particularly important. In the high-incident-energy region, the rearrange amplitudes are appreciable and the capture amplitudes may be neglected.

In Fig. 6, we display the reduced total cross section for Li^+ compared with the theoretical calculations of Economides and McDowell [6], Moores and Nussbaumer [7], Younger [10], and Pindzola *et al.* [15] and with the experimental data of Lineberger *et al.* [25], Wareing and Dolder [26], and Peart and Dolder [27]. The TPDW01 and TPDW11 curves give better results than the TPDW00 curve at high

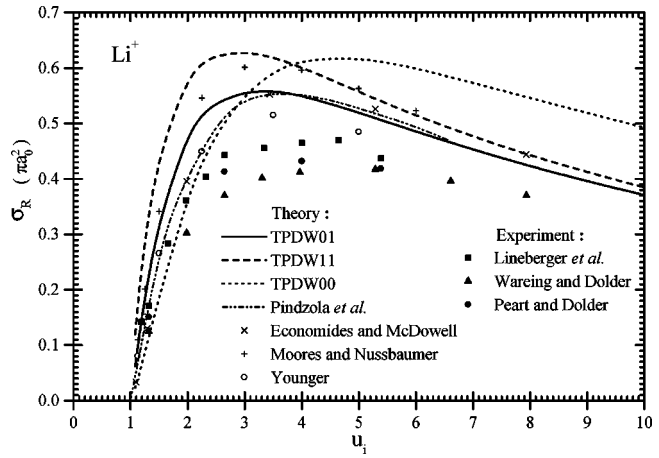

FIG. 6. Reduced total cross sections (in πa_0^2) for Li^+.

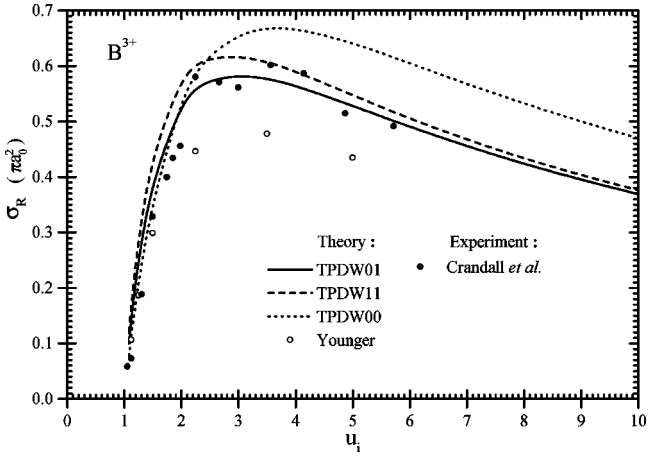

FIG. 7. Reduced total cross sections (in πa_0^2) for B^{3+}.

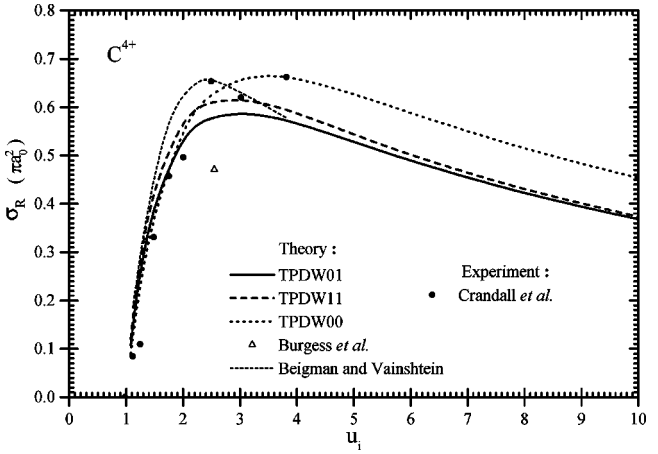

FIG. 8. Reduced total cross sections (in πa_0^2) for C^{4+}.

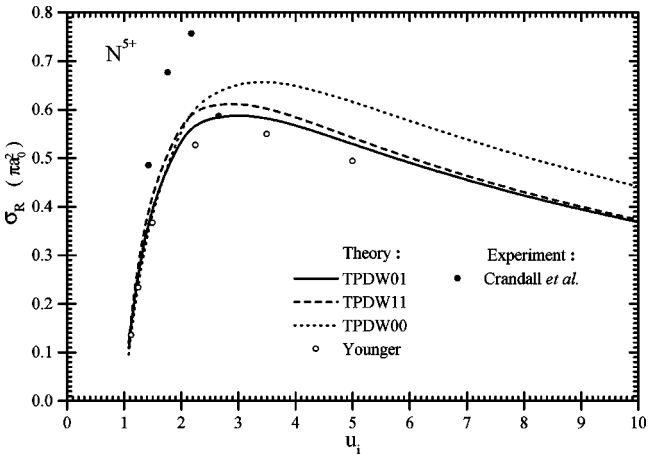

FIG. 9. Reduced total cross sections (in πa_0^2) for N^{5+}.

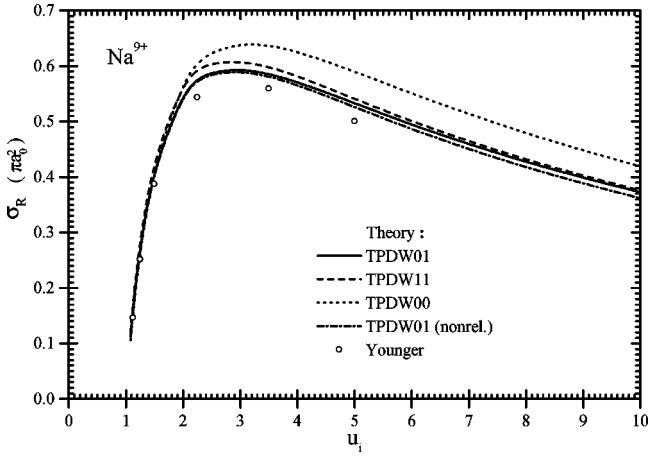

FIG. 10. Reduced total cross sections (in πa_0^2) for Na^{9+}.

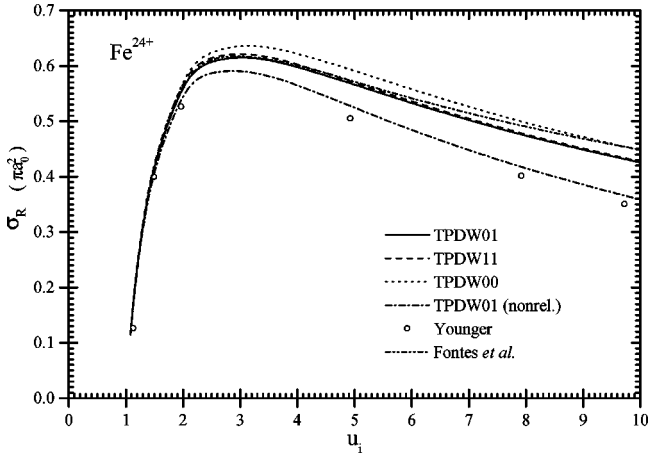

FIG. 11. Reduced total cross sections (in πa_0^2) for Fe^{24+}.

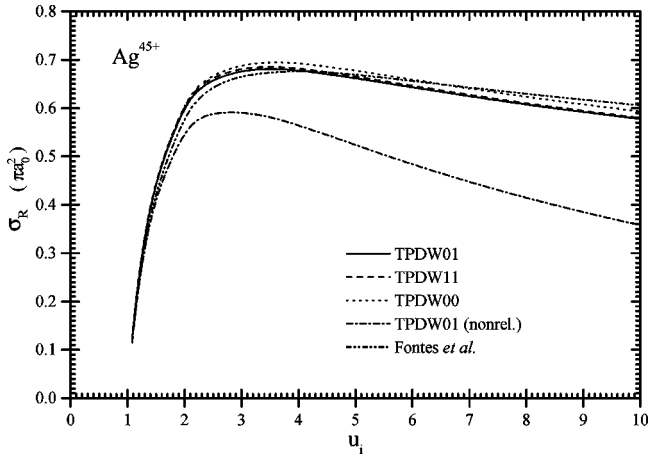

FIG. 12. Reduced total cross sections (in πa_0^2) for Ag^{45+}.

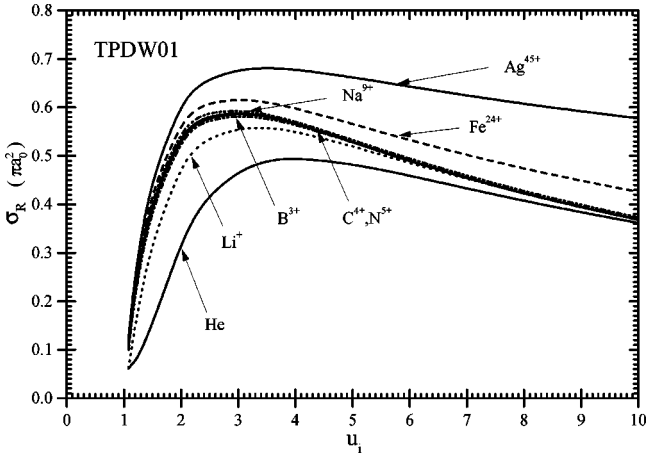

FIG. 13. Reduced total cross sections (in πa_0^2) in model TPDW01 for $He,Li^+,B^{3+},C^{4+},N^{5+},Na^{9+},Fe^{24+},Ag^{45+}$.

incident energies. At low incident energies, the primary and secondary electrons have small available kinetic energies and should be strongly screened by each other, so that the TPDW00 curve gives slightly better results.

In Fig. 7, we show the reduced total cross section for B^{3+} and compare with that of Younger [10] and with the experimental data by Crandall *et al.* [28]. Like the Li^+ case, the TPDW00 curve is in better agreement with experiment at low u_i, and the TPDW01 and TPDW11 curves give better results at high u_i. In Fig. 8, we show the reduced total cross section for C^{4+} in comparison with theoretical calculations of Burgess *et al.* [8] and Beigman and Vainshtein [4] and with the experimental data by Crandall *et al.* [28]. We display the reduced total cross sections for N^{5+} and Na^{9+} in Figs. 9 and 10, respectively, and compare them with the nonrelativistic calculations of Younger [10] and with the experimental data of Crandall *et al.* [28]. As shown in Fig. 10, the nonrelativistic TPDW01 values are slightly lower than the relativistic TPDW01 values at high incident energies for Na^{9+}. In Fig. 11, we present the reduced total cross section for Fe^{24+} and compare with the corrected results of Younger [11] as explained by Fontes *et al.* [40] and with the interpo-

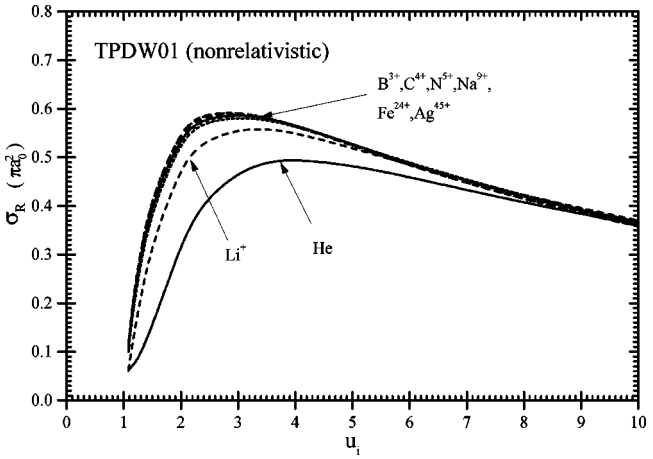

FIG. 14. Nonrelativistic reduced total cross sections (in πa_0^2) in model TPDW01 for $He,Li^+,B^{3+},C^{4+},N^{5+},Na^{9+},Fe^{24+},Ag^{45+}$.

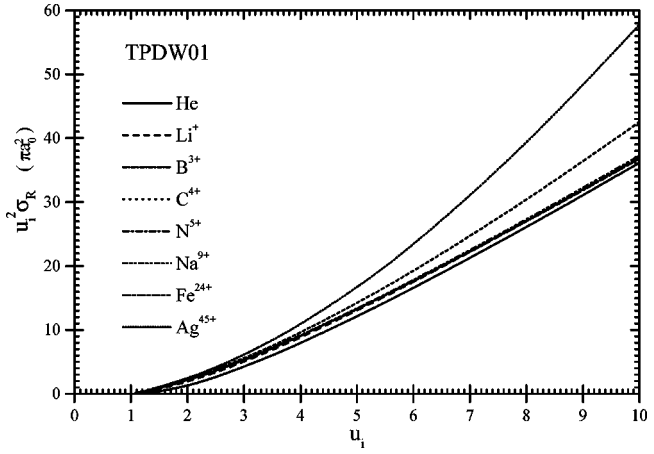

FIG. 15. Reduced total cross sections multiplied by u_i^2 (in πa_0^2) in model TPDW01 for He,Li^+,B^{3+},C^{4+},N^{5+},Na^{9+},Fe^{24+},Ag^{45+}.

lated results of Fontes *et al.* by their fitting formula [14]. The difference between our results and that of Fontes *et al.* indicates the importance of the Breit interaction effects. The TPDW01 and TPDW11 curves are hardly discernible from each other at high u_i. The reduced total cross section of Ag^{45+} are shown in Fig. 12, with the fitting-formula results of Fontes *et al.* [14], and there is not much difference among our three models. From Figs. 11 and 12, we note that the relativistic and Breit-interaction effects are evident for highly charged ions.

To examine the systematics of electron-impact ionization along the helium isoelectronic sequence, we plot the TPDW01 curves for all ions in Fig. 13. Here all curves seem to follow a universal trend, rising sharply near the threshold and decreasing gradually at high incident energies. The departure of the He and Li^+ curves is due to correlation effects, while the departure of the Fe^{24+} and Ag^{45+} curves is due to relativistic effects in ions of high nuclear charge. In Fig. 14, we present the nonrelativistic TPDW01 curves, the universal trend is more apparent. The reduced total cross sections multiplied by u_i^2 are presented in Fig. 15 for the TPDW01

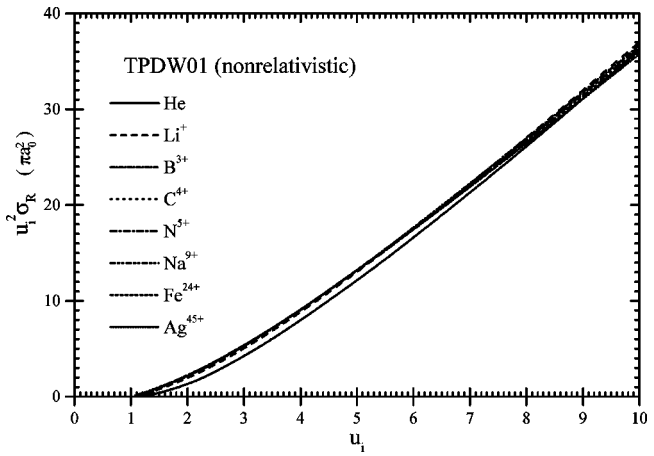

FIG. 16. Nonrelativistic reduced total cross sections multiplied by u_i^2 (in πa_0^2) in model TPDW01 for He,Li^+,B^{3+},C^{4+},N^{5+},Na^{9+},Fe^{24+},Ag^{45+}.

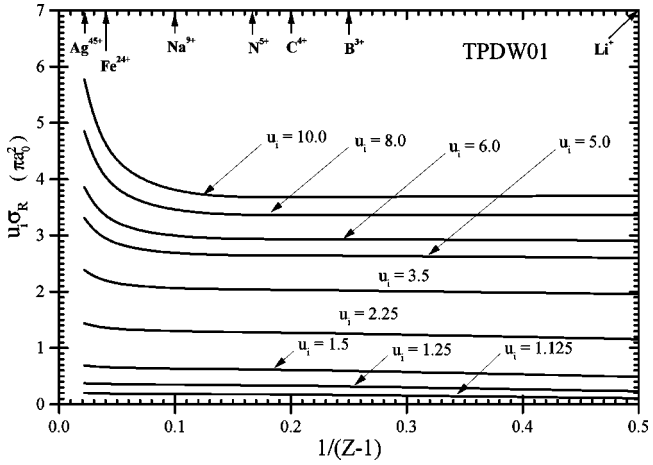

FIG. 17. Isoelectronic plot of reduced total cross sections multiplied by u_i (in πa_0^2) in model TPDW01. Here Z denotes the nuclear charge. Each curve corresponds to an incident energy u_i (in threshold energy units).

model. Here again, we find that the deviation of the He and Li^+ curves from the universal trend is due to correlation effects, and the obvious deviation of the Fe^{+24} and Ag^{+45} curves is due to the relativistic effects. In Fig. 16, we show the corresponding results in the nonrelativistic limit, all curves converge to a universal curve and to become almost a straight line except near the threshold.

So far we only consider the reduced total cross sections plotted against the incident energies. To study the systematic behavior of the helium isoelectronic sequence at fixed incident energies, we present the scaled cross sections $u_i\sigma_R$ versus the inverse of effective ion charges $(Z-1)$ in Fig. 17 for the TPDW01 model. In this way, we can easily interpolate or extrapolate data of new ions from existing curves. We find that these curves rise sharply for highly charged ions at high incident energies because of the relativistic effects. However, the Breit-interaction effects, which are not accounted for in the present approach, may significantly increase the ionization cross sections for high Z ions as demonstrated by Fontes

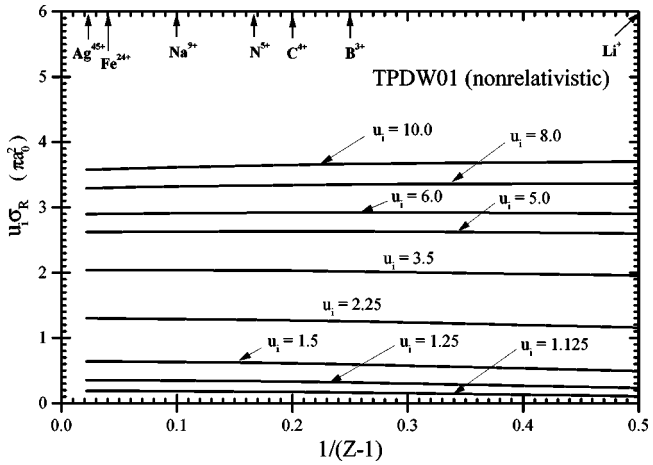

FIG. 18. Isoelectronic plot of nonrelativistic reduced total cross sections multiplied by u_i (in πa_0^2) in model TPDW01. Each curve corresponds to an incident energy u_i (in threshold energy units).

et al. [14]. The nonrelativistic scaled cross sections $u_i\sigma_R$ are plotted in Fig. 18, in which each nonrelativistic curve at fixed u_i appears as a horizontal line.

V. CONCLUSION

A fully relativistic calculation of the electron-impact ionization cross sections for heliumlike ions is performed. We compute the transition amplitudes in the two-potential distorted-wave approximation with exact exchange effects. The exchange, including rearrange and capture, amplitudes are found to be important. Three different sets of asymptotic charges in three models, TPDW01, TPDW11, and TPDW00, are used for the distorting potentials to study the mutual screening of the primary and secondary electrons. The relativistic effects are studied by comparison with ionization cross sections in the nonrelativistic limit. We conclude that correlation effects are important for lower-Z ions and the relativistic effects are prominent for higher-Z ions. Our results along the helium isoelectronic sequence follow a systematic trend and agree well with available theoretical and experimental results. Cross sections for other ions of interest along the helium isoelectronic sequence may be interpolated or extrapolated from the existing data. In addition, one should also consider the Breit-interaction effects, which have been shown by Fontes *et al*. [14] to be important for high Z and/or high impact energies.

ACKNOWLEDGMENT

This work was supported in part by the National Science Council of the Republic of China under Grant No. NSC89-2112-M001-065.

[1] I.E. McCarthy and E. Weigold, Phys. Rep. **27C**, 275 (1976).
[2] T.D. Mark and G.H. Dunn, *Electron Impact Ionization* (Springer, Wien, 1985).
[3] H. Tawara and T. Kato, At. Data Nucl. Data Tables **36**, 167 (1987).
[4] I.L. Beigman and L.A. Vainshtein, Astron. Zh. **11**, 712 (1968).
[5] K.L. Bell and A.E. Kingston, J. Phys. B **2**, 1125 (1969).
[6] D.G. Economides and M.R.C. McDowell, J. Phys. B **2**, 1323 (1969).
[7] D.L. Moores and H. Nussbaumer, J. Phys. B **3**, 161 (1970).
[8] A. Burgess, H.P. Summers, D.M. Cochrane, and R.W.P. McWhirter, Mon. Not. R. Astron. Soc. **179**, 275 (1977).
[9] B.H. Bransden, J.J. Smith, and K.H. Winters, J. Phys. B **12**, 1267 (1979).
[10] S.M. Younger, Phys. Rev. A **22**, 1425 (1980).
[11] S.M. Younger, J. Quant. Spectrosc. Radiat. Transf. **26**, 329 (1981).
[12] Y.-K. Kim and M.E. Rudd, Phys. Rev. A **50**, 3954 (1994).
[13] R. Biswas and C. Sinha, Phys. Rev. A **54**, 2944 (1996).
[14] C.J. Fontes, D.H. Sampson, and H.L. Zhang, Phys. Rev. A **59**, 1329 (1999).
[15] M.S. Pindzola, D.M. Mitnik, J. Colgan, and D.C. Griffin, Phys. Rev. A **61**, 052712 (2000).
[16] J.T. Grissom, R.N. Compton, and W.R. Garrett, Phys. Rev. A **6**, 977 (1972).
[17] C.D. Opal, E.C. Beaty, and W.K. Peterson, At. Data **4**, 209 (1972).
[18] J.B. Crooks, Ph.D. thesis, University of Nebraska, 1972.
[19] T.W. Shyn and W.E. Sharp, Phys. Rev. A **19**, 557 (1979).
[20] P.T. Smith, Phys. Rev. **36**, 1293 (1930).
[21] B.L. Schram, F.J. de Heer, M.J. Van der Wiel, and J. Kistelmaker, Physica **31**, 94 (1964).
[22] E. Brook, M.F.A. Harrison, and A.C.H. Smith, Culham Report, 1978 (unpublished).
[23] R.G. Montague, M.F.A. Harrison, and A.C.H. Smith, J. Phys. B **17**, 3295 (1984).
[24] M.B. Shah, D.S. Elliott, P. McCallion, and H.B. Gilbody, J. Phys. B **21**, 2751 (1988).
[25] W.C. Lineberger, J.W. Hooper, and E.W. McDaniel, Phys. Rev. **141**, 151 (1966).
[26] J.B. Wareing and K.T. Dolder, Proc. Phys. Soc. London **91**, 887 (1967).
[27] B. Peart and K.T. Dolder, J. Phys. B **1**, 872 (1968).
[28] D.H. Crandall, R.A. Phaneuf, and D.C. Gregory, Oak Ridge National Laboratory Report No. ORNL/TM-7020, 1970 (unpublished).
[29] K.-N. Huang, Phys. Rev. A **28**, 1869 (1983).
[30] K.-N. Huang, Chin. J. Phys. (Taipei) **25**, 156 (1987).
[31] T.-Y. Kuo, Ph.D. Thesis, National Taiwan University, 1987.
[32] H.-C. Kao, T.-Y. Kuo, H.-P. Yen, C.-M. Wei, and K.-N. Huang, Phys. Rev. A **45**, 4646 (1992).
[33] S.-W. Hsu, T.-Y. Kuo, C.-M.J. Chen, and K.-N. Huang, Phys. Lett. A **167**, 277 (1992).
[34] T.-Y. Kuo, C.-M.J. Chen, S.-W. Hsu, and K.-N. Huang, Phys. Rev. A **48**, 357 (1993).
[35] J.-C. Chang, C.-M. Wei, T.-Y. Kuo, and K.-N. Huang, J. Phys. B **27**, 4715 (1994).
[36] K.-N. Huang, W.-Y. Cheng, and T.-Y. Kuo, J. Korean Phys. Soc. **32**, 232 (1998).
[37] M. L. Goldberger and K. M. Watson, *Collision Theory* (Wiley, New York, 1965), Chap. 5.
[38] J.P. Desclaux, Comput. Phys. Commun. **9**, 31 (1975).
[39] K.-N. Huang, Rev. Mod. Phys. **53**, 215 (1979).
[40] C.J. Fontes, D.H. Sampson, and H.L. Zhang, At. Data Nucl. Data Tables **72**, 217 (1999).